International Journal of Engineering Research and General Science Volume 5, Issue 3, May-June, 2017
ISSN 2091-2730

STUDY OF MATHEMATICS INVOLVED IN GAS ATOMISATION PLANTS AND SPRAY FORMINGS

Pankaj Sharma
Assistant Professor
Department of Mechanical Engineering
B S Dr B R A College of Agril Engg & Tech,
Etawah – 206001 (UP), INDIA
Email: pankajsharma1437@gmail.com

ABSTRACT- In Spray forming processes, a continuous molten metal stream is atomized by impinging a very high speed inert gas jets. The velocity of jet is very high to atomised the molten liquids. In the generated spray cone, the resulting metal droplets are rapidly cooled by the huge temperature difference to the surrounding gas phase and thereby partly solidify. After a certain flight and residence time inside the spray cone, the droplets impinge on the substrate and form the product sometimes called deposit. The material properties of this product depend on several process parameters and especially on the thermal state of the deposited droplets at impingement. Smaller droplets cool very fast and may impinge onto the product in a completely solidified state as solid metal powder particles. Larger droplets contain a higher amount of thermal energy and impact during the state of phase change or even still completely liquid. In this contribution, a mathematical model is introduced to describe the cooling and solidification of individual metal droplets in the spray cone during the droplet–gas interaction in flight. By introducing this model into a standard two phase flow simulation model for the spray cone description, it is possible to calculate the transient droplet temperature and solid fraction contents of individual particles depending on overall process parameters and flight path.It is very important to study mathematics involved in the metal forming processes only because of it we enable to predict the thermal behaviour of the spray formed products.

1. INTRODUCTION

In recent years spray formings have been an emerging forming process for the production of near net shape products with the benefits that of rapid solidification, semi solid processing etc. This spray forming processes combine the advantage of metal casting and powder metallurgy. Spray forming has minimized the multiple steps of powder metallurgy which includes processes like powder production, sieving, de-gasing and consolidation into a single processing step and still micro-structural characteristics remains the same. Figure 1, illustrates the schematic view of spray forming.

Professor Singer at the Swansea University first developed the idea of gas atomized spray forming in 1970s in which a high pressure gas jet impinges on a stable melt stream to cause atomization. The resulting droplets are then collected on a target, which can be manipulated within the sprays and used to form a near-dense billet of near-net shape Spray forming, also known as spray casting, spray deposition is a method of casting near net shape metal components with homogeneous microstructures via the deposition of semi-solid sprayed droplets onto a shaped substrate. In spray forming an alloy is melted, normally in an induction furnace, then the molten metal is slowly poured into a conical tundish into a small-bore ceramic nozzle. The molten metal exits the furnace as a thin free-falling stream and is broken up into droplets by an annular array of gas jets, and these droplets then proceed downwards, accelerated by the gas jets to impact onto a substrate. 'The process is arranged such that the droplets strike the substrate whilst in the semi-solid condition, this provides sufficient liquid fraction to 'stick' the solid fraction together. Deposition continues, gradually building up a spray formed billets of metal on the substrates.

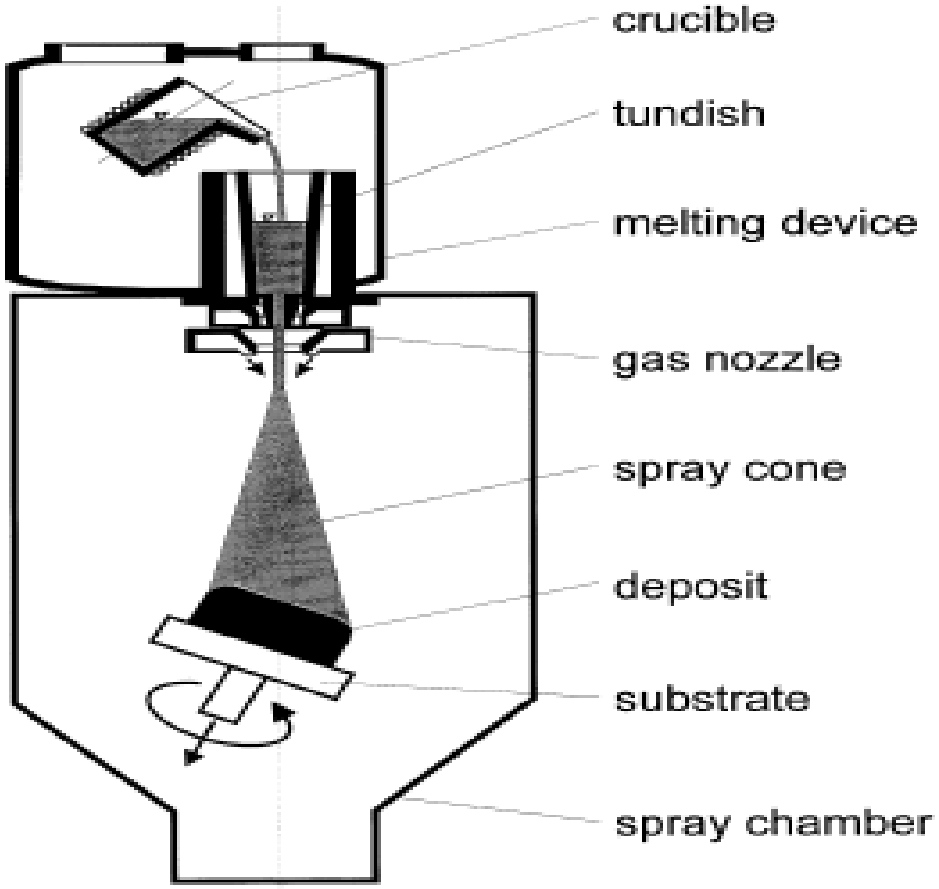

FIGURE 1.1 Schematic view of spray forming processes

In the spray forming processes the metal is heated in the crucible until the superheat temperature is reached and the molten metal is poured in the tundish. The molten metal stream is poured into the atomization chamber using the gravity, where the molten metal stream gets disintegrated into spherical droplets due to jets of inert gases with very high kinetic energy. The spray thus formed gets accelerated towards the preformed substrate, cools down and solidifies partly as a result of high rate of heat transfer from the spray to the cold inert gas. The diameters of gas atomized droplets varies from 5µm to 500µm. Later on the droplets impacts on to the substrate, merges and forms the deposit.

It was in 1960 in Swansea, Wales, by Singer and his colleagues when the first use of metal spray forming was used. In 1970s, spray forming was used as a substitute for conventional forming as production of preform was done directly from the melt. The spray forming process for money-making was first used by a number of singer's young researchers and as a result of which they founded the company Osprey Metals in Neath, Wales. Hence sometimes spray forming process is also called as the Osprey process. Since then, application potentials of the spray forming process has ignited several research and development works at universities and at various industries. In the late '80s Lavernia and Grant developed the liquid dynamic compaction (LDC) process which was similar to spray forming. LDC, Osprey process and spray formings are the generic names of similar or related processes.

2. SUBDIVISION OF SPRAY FORMING PROCESSES

From the process technology view point spray forming is divided into many sub processes. The subdivision of the complete spray forming is shown in fig 2.1.

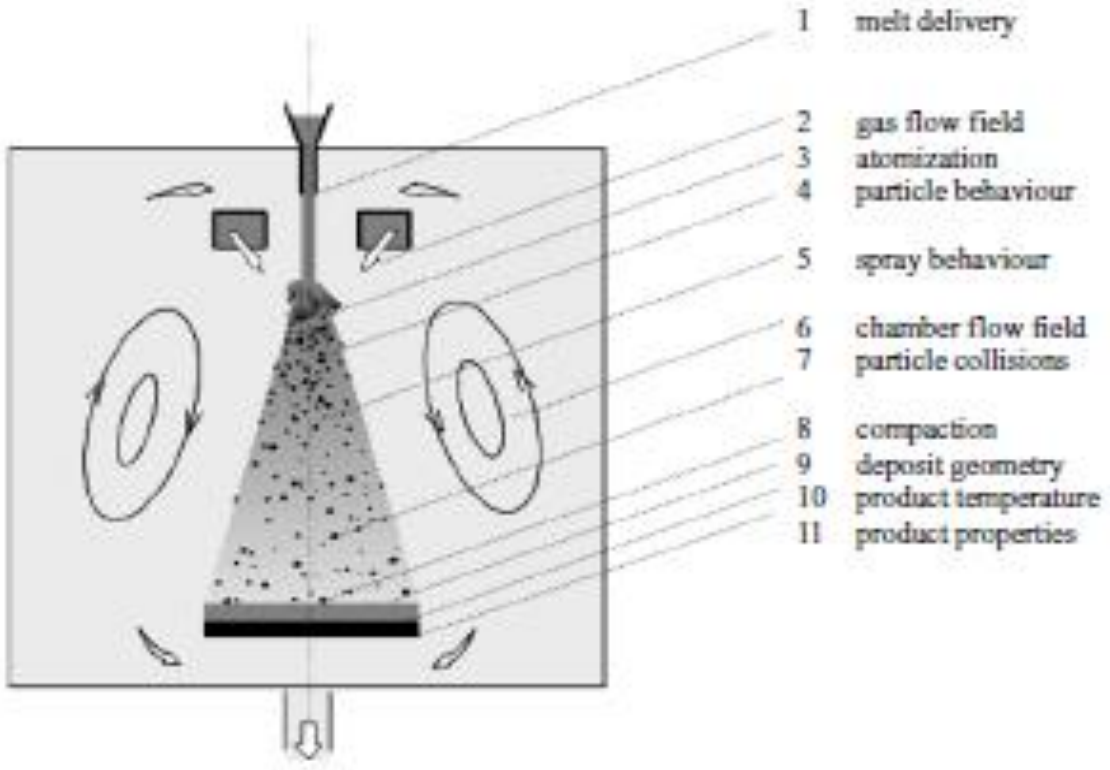

FIGURE 2.1 Sub process view of spray forming.

The spray structure consists of in-flight accelerated, thus cooled and partially solidified, melt droplets as well as rapidly heated and decelerated gas flow. Analysis of individual droplet is done to know the behavior regarding movement and cooling of the droplet.

Ojha *et al* described the reason of why analysis of droplet is done before they impinge onto the substrate and is shown as under:-

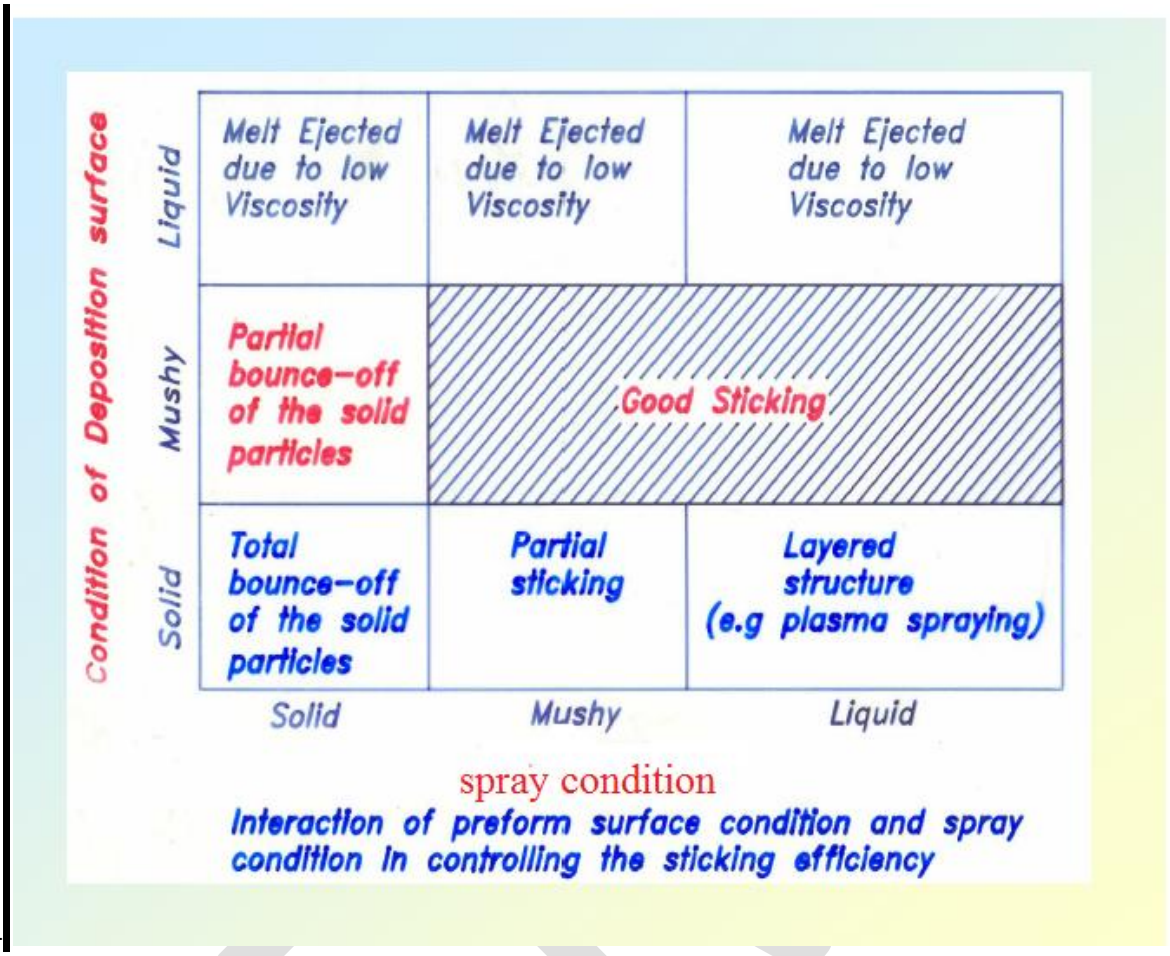

TABLE 2.1:Interaction of peform surface condition and spray condition in controlling in controlling the sticking efficiency

Lawley *et al* (1990) and Mathur *et al.* (1991) have inspected the spray forming process, and have discovered how fundamental knowledge of atomization and the compaction processes affect the system construction. In this way it was found that the appropriate control of processes parameters, such as substrate movements, sprays oscillation, deposit temperature and so on is must, as shown in figure 2.2. This diagram consists of process that can be controlled by operator on the left side and processes that cannot be controlled by operator directly and the bottom consist of the spray conditions at impact and the surface conditions of the substrate/deposit.

The main purpose of Lawley *et al*.'s and Mathur *et al.*'s was to know parameter that can be controlled and they found that the significant parameters are

- Geometry and dimension of deposits
- The microstructures of the final product (porosity and grain size).

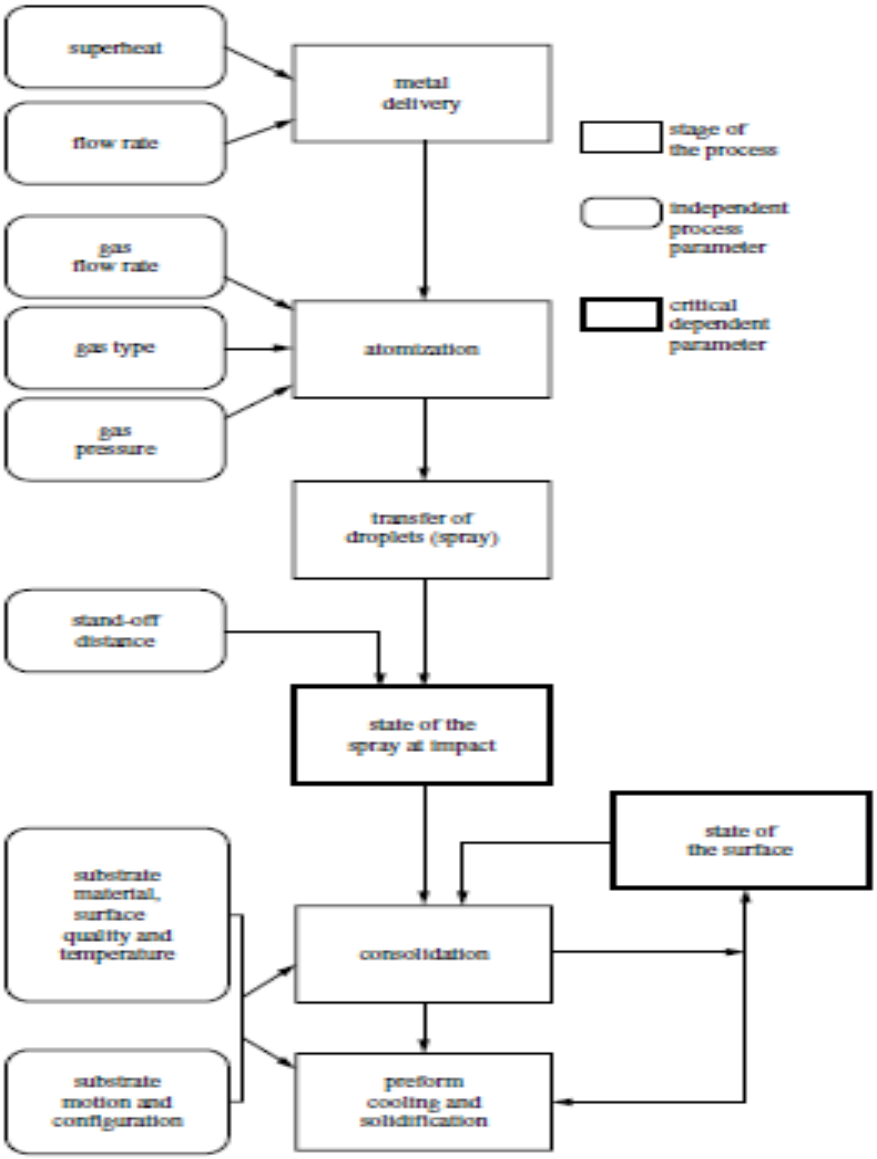

FIGURE 2.2 Modelling of independent & dependent process parameters

In his work, **Ottosen (1993)** identified the main function in analysis of an integral spray forming model was the modelling and simulation of complex heat transfer and momentum exchange processes.

Bauckhage and Uhlenwinkel (1996) laid emphasis on automated and optimized spray forming process, by dividing the spray formings in 3 parts which are melting and atomization, particles transport in spray and compaction.

The process parameters and product quality was linked by **Payne *et al* (1993*)*** by the empirical spray forming process model. For suitable process control, Payne *et al* has recognized:

- Process parameters controlled directly: e.g. spray time, melt temperature and GMR;
- Indirectly controllable process parameters: e.g. exhaust gas temperatures, deposit surfaces, roughness and porosity.

The multi-coupled simulation of turbulent dispersed multiphase flow, containing gas as a continuous phase and droplets as a dispersed phase, is based on two modeling concepts:

- Eulerian/Lagrangians approach

This approach is related to direct intuitive approach which is applied in the analysis of the behavior of dispersed multiphase flow. In this individual particle is under the scanner of study and its interaction with local surroundings are analyzed on the scale of droplets size. **Crowe *et al* (1977), Grant *et al* (1993), Bergmann *et al* (1995)** were the researchers who published several models within spray formings application based on this approaches.

- Eulerian/Eulerians approach

In this the dispersed phase is considered to be as a quasi-second fluid with spatially averaged properties. Based on this approach derivation of the spray structure within the spray forming process has been done by **Liu (1990) and Fritsching *et al* (1991).**

3. Particle Movement

A fundamental description of the behavior of droplets in gas, the flow around gas atomized droplets and their analysis is given in **Clift et al (1978), Crowe et al (1998), Sadhal et al (1997) and Sirignano (1999).**

The various forces exerted on individual spherical particles are listed in table 3.1.

(1) inertial force	$F_i = -\rho_p V \frac{dv_p}{dt}$
(2) field force	
• gravity force	$F_g = \rho_p V g$
(3) pressure forces	
• buoyancy force	$F_a = -\rho_g V g$
• pressure gradients	$F_p = -\rho_g \frac{dv_g}{dt} V$
(4) fluid mechanics forces	
• resistance force	$F_w = -\frac{1}{2}\rho_g A_p c_w(\mathrm{Re})\lvert v_p - v_g\rvert(v_p - v_g)$
• added mass	$F_m = -\frac{1}{2}\rho_g V\left(\frac{dv_p}{dt} - \frac{dv_g}{dt}\right)$
(5) other forces	
• Basset history integral	$F_b = \frac{3}{2}d^2\sqrt{\frac{\rho_g \mu}{\pi}}\left(\int_{-\infty}^{t} \frac{\frac{dv_p}{d\tau} - \frac{dv_g}{d\tau}}{(t-\tau)^{1/2}} d\tau + \frac{(v_p - v_g)_0}{\sqrt{t}}\right)$

TABLE 3.1:Various forces acting on droplets

The spherical droplet trajectory is derived from: ∑F=O

The added-mass term describes the involvement of the surrounding gas, which gets accelerated together with the particle in the boundary layer of the particle. The last term of Basset history integral has been discovered by **Reeks and McKee (1984)** for the finite particle starting velocity.

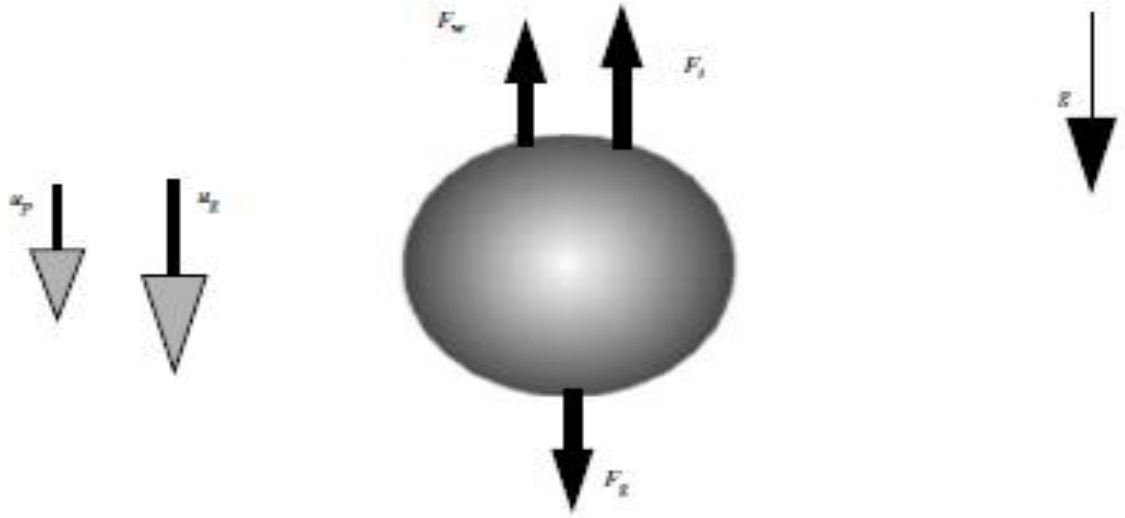

FIGURE 3.3 Coordinate system for force-balancing for spherical droplet

In the analysis of gas atomized droplets, the density ratio of gas to the particles is negligible ($\rho_g/\rho_p < 10^{-3}$). The particle trajectory equation can be simplified:

$$m_p\frac{\partial U_p}{\partial t}=m_pg+\frac{1}{2}p_gIu_g-u_pI(u_g-u_p)C_dA_p \qquad (3.1)$$

The force balance taken into account are force due to inertia, gravity and resistance. The resistance drag force coefficients c_d is described in the range of Reynolds number.

Re < 800

$$C_d=\frac{24}{Re}(1+0.15Re^{0.687}),\ Re< 800 \qquad (3.2)$$

Cliff *et al* (1978) found that in the area of stokes flow Re <1,

$$C_d=\frac{24}{Re}\left(\frac{1+\frac{2}{3}\mu}{1+\mu}\right) \quad Re< 1 \qquad (3.3)$$

N S MAHESH *et al* (2002) investigated the influences of dynamics of the droplets and temperature variations on the microstructures of final products. For this analytical models were constructed taking into consideration higher Reynolds number leading to supersonic flow of gases. The nozzles were designed so as to develop Mach no 3. Figure 2.4 describes the variation of velocity profile with flight distance. Initial gas velocity was put = 1000.00 m/s. It was seen that the gas velocity decays exponentially with respect to flight distance and reaches 200 m/s at a distance of 0.7 m from the region of atomization. Although it was not enough to provide information on the impact velocity of the droplet but it was the first step for computing droplet velocity. In the present study, instead of considering a constant velocity (or average velocity), instantaneous gas velocity obtained from gas velocity plot was used to obtain

droplet velocity profile for different size droplets. This provided more realistic droplet velocity and increases the accuracy of the model.

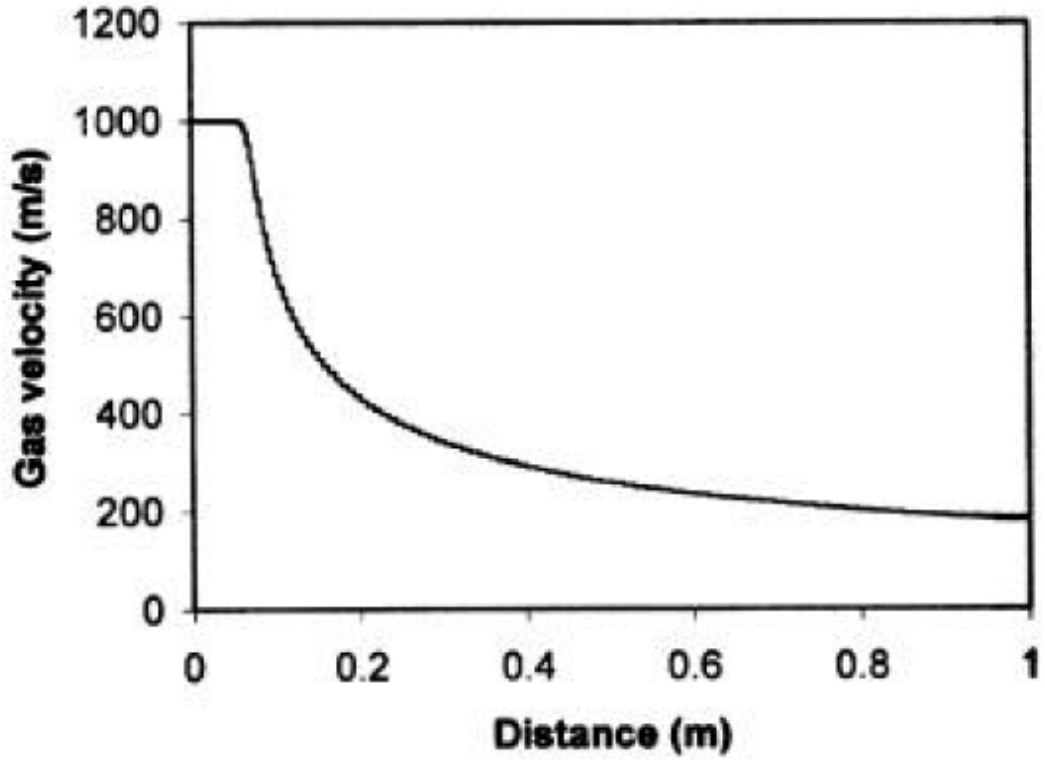

FIGURE 3.4 Variation of gas velocity with respect to the flight distance

Figure 3.5 shows the graph between Reynolds number and the flight distance for different droplets sizes computed based on the relative velocity of the gas and droplets. It is obvious from the graph that the Reynolds number for the larger droplets is more predictable, as the Reynolds number is directly proportional to the droplet diameter. Reynolds number for the entire chosen droplet sizes was more than 4000 in the present study.

$Re = \rho.u.d/\mu$

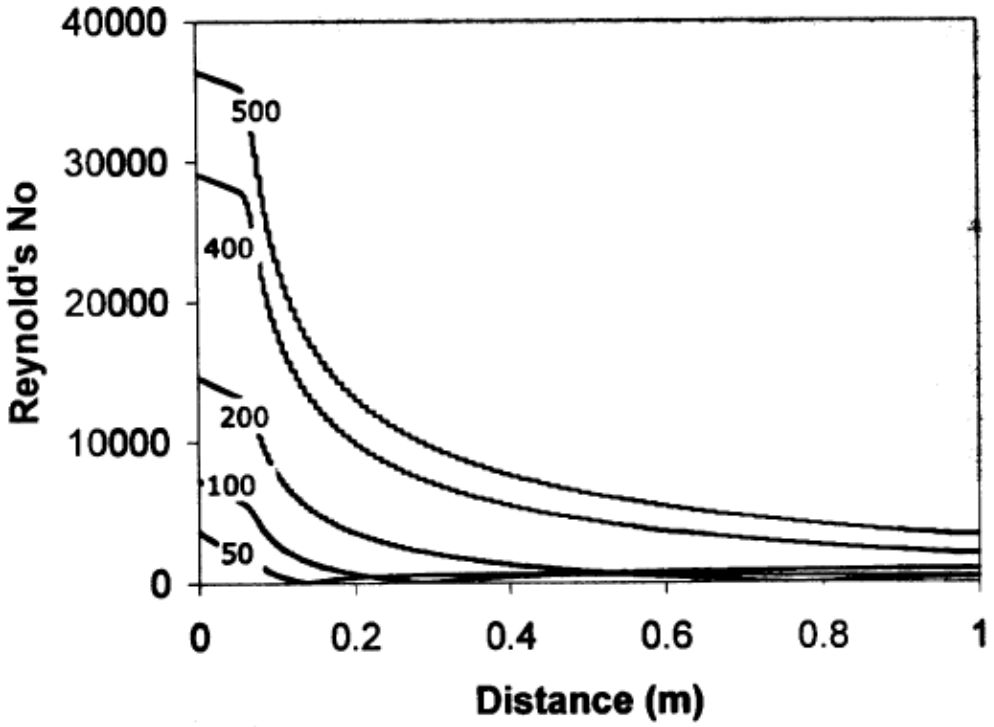

FIGURE 3.5 Variation of Reynolds number for different droplet size

Figure 3.6 shows the droplet's and gas velocity profile for varying sized droplets with respect to flight distance. It is obvious from the graph that at the exit of the nozzle the droplets have very less velocity (equal to acceleration due to gravity) and during the flight they gain velocity owing to the momentum transfer from the atomizing gases. The smallest droplet attains highest velocity during the flight and *vice versa*.

The relative velocity of gas and droplet becomes zero as the flight distance increases and is equivalent to Reynold numbers variation.

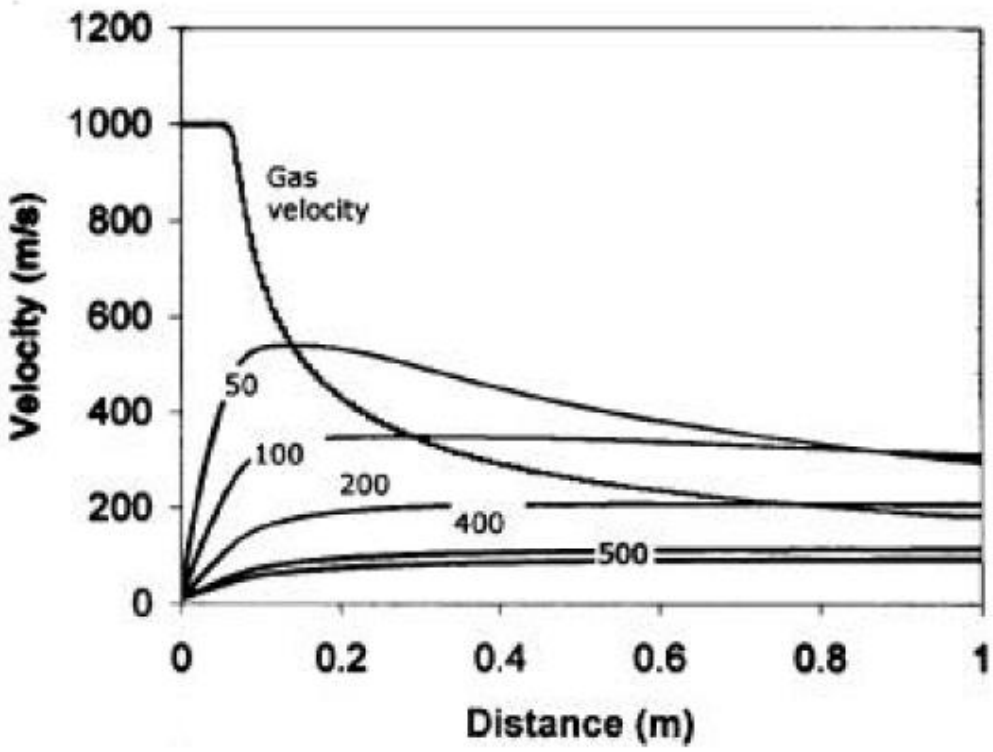

FIGURE 3.6 Droplet's and Gas Velocity Profile for Varying Sized Droplets With respect to Flight Distances

The smaller droplets moves faster than atomizing gas and attain maximum velocity in minimum time. As the Reynolds number for smaller droplets are extremely small, the drag forces are large. As a result smaller droplets are decelerating faster and show noticeable peak velocity. On the other hand, the drag coefficients for the larger droplets is approximately constant after the peak velocity due to their high inertia forces and thus no deceleration happens. Most of the droplets are at considerably high velocity (> 100 m/s) while they impinge to the substrate. It has been proposed by various investigators that dendrite fragmentation mechanism is best to explain equiaxed grain morphology since mushy (semi-solid/semi-liquid) droplet reach the substrate with considerable velocity. In the present analysis a possibility for dendrite fragmentations are evident from the droplet-velocity plots.

4. Heat transfer and Cooling of the droplet

The microstructure and the properties of sprayed alloy or of the final product can be known approximately by calculating the droplet thermal histories **(Gutierrez *et al* 1988; Lavernia *et al* 1988)**. The cooling due to convection is largely responsibles for heat transfer in metal droplets because of a large temperature differences between molten metal droplets and cool atomizing gas. As a result for liquid metal droplets during atomization, convective cooling dominates over radiative cooling and hence radiation effect can be neglected **(Lavernia *et al* 1988; Mathur *et al* 1989; Grant *et al* 1993; Eon-Sik Lee and Ahn 1994)**. However, since the heat extractions from a droplets surface depends on the relative velocity between the cooling gas and the droplet itself, it is necessary to estimate droplet and gas velocities as discussed by **Lavernia *et al* (1988)**.

Most of the researchers have adopted lumped parameter models (LPM) for calculation of heat transfer in gas atomized droplets (Lavernia *et al* 1988; Mathur *et al* 1988; Gutierrez *et al* 1989; Grantt *et al* 1993; Eon-Sik Lee and Ahhn 1994; Dimos and John 1997). Moreover, **Levi and Mehrabian (1982)** shows that LPM give needed results when the temperature gradient inside the droplet is very large. The LPM is used for the simplicity of computation, since only first order ordinary differentials equations are to be solved. The small size of the droplets play a significant role in neglecting the heat conduction within

the droplets i.e**. the droplet temperature is considered uniform (Lavernia *et al* 1988; Grant *et al* 1993; Eon/Sik Lee and Ahn 1994)**.

The process of conduction freezing using LPM as well as radially symmetric non-isothermal models have been analyzed by **(Bayazitoglu and Cerny 1993)**. In this not only the radial symmetry was imposed on the droplet but also the presence of recalescence resulting from severe undercoolings and phenomena of non-equilibrium was neglected. The LPM is accurate and also the assumption of uniform temperature inside the droplet is justified when the cooling rate was 104K/s. This follows the Newtonian cooling and gives rise to LPM.

Now equating the rate of change in surface of the sensible heat contained in the droplets to the rate of heat extraction through the outer surface of the droplets **(Lavernia *ett al* 1988),**

$m_p c_p \frac{dTp}{dt} = Nu\ \lambda g \pi d_p (Tg-Tp)$ (4.1)

Equation (4.2) can be readily integrated if heat transfer coefficient, *h*, is assumed to be constant. But heat transfer coefficients could not be considered to be a constant since the velocity of the gas decreases and that of the droplets increases. Since radiation effects can be neglected, the heat transfer coefficient '*h*' is calculated using **(Ranzz and Marshal 1952).**

$Nu=2+0.6Re^{0.5}Pr^{0.33}$ (4.2)

$Pr = \frac{C_g \mu_g}{K_g}$ (4.3)

Where, *C*g is the gas specific heat, μ_g the absolute viscosity of gas and K_g the gas thermal conductivity

Equation (4.2) represents Nusselt numbers given by (Ranz and Marshall 1952) correlation for laminar convection from a solid sphere. The Nusselt numbers is depends on droplet diameter, the surface averaged heat transfer coefficient between the gas and the droplets and the free-stream thermal conductivity. The Prandtl numbers is that of the gas at free-stream conditions. The Reynolds number is based on the relative velocity between the droplets and the free-stream. Here it is important to note that the Ranz and Marshal correlation used by many researchers **(Lavernia *et-al* 1988; Mathur *et al* 1989; Grant *et al* 1993; Eon/Sik Lee and Ahn 1994)** has limited validity **(Dimos and John 1997)**. As the Ranz and Marshall's correlation for '*h*' is correct when the Reynolds number lies in the range of 0.1 to 4000. For supersonic gas atomization when Remore than 4000 Whitaker's (1972) correlation is used:

$Nu = \frac{hD}{K} = 2+(0.4Re^{1/2}+0.06Re^{2/3})\ Pr^{0.4}(\frac{\mu_{00}}{\mu_s})$ (4.4)

Heat transfer coefficient with the function of flight distanced is to be known first before predicting the thermal states of droplets. For this Whitaker's correlation for heat transfer from isothermal spherical surface was incorporated in the software code to obtain heat transfer coefficient plots. From figure 7 it can be shown that the smaller droplets would have larger heat transfer rate since they have larger surface area to volume ratio. The instantaneous heat transfer coefficients was used for obtaining thermal history of droplet.

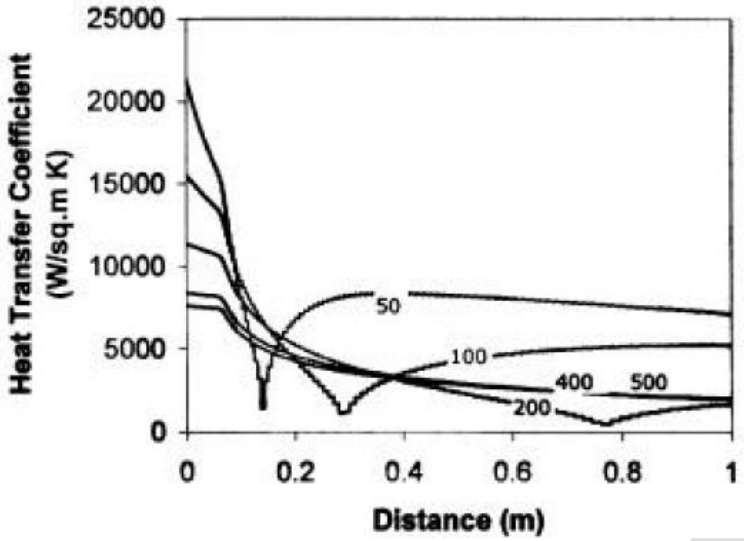

FIGURE 4.1 the variations in heat transfer coefficients for different droplet size with the flight distance

Figure 4.2 shows temperature variation for different droplet sizes as a functions of flight distance. The solidus and liquidus temperature are illustrated to identify the physical state of the droplets based on their size when they reach the substrate. We know that mushy droplets provide best quality preform hence it is important to know which droplet size strike the substrate in mushy zone and it was done by determining solid fraction of droplet.

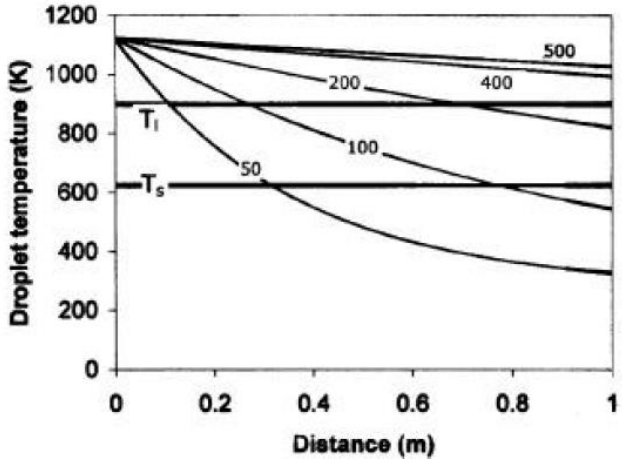

FIGURE 4.2 temperature variation for different droplet sizes as a function of flight distances

Figure 4.3 depicts percentage of solid in the droplets versus flight distance. It is seen from the figure that smaller droplets solidify completely at a distance from 0.2 to 0.6 m. The droplets of more than that of 100 µm sizes would be in semi solid/semi liquid state for a longer time. This analysis helps in optimizing the stand-off distances for given set of atomization parameters and for a particular metal and its alloys system. From this analysis it was found that the standoff distance of 0.6 to 0.7 m is suitable for obtaining preform in Al–Si–Mg alloy during the deposition trials. At this standoff distance it was anticipated that the droplets of size variety between 100 and 500 µm possesses 90% to 15% solid fractions respectively. The parameters in spray casting be set up in such a way that the spray has more volume fraction of mushy droplets i.e. the droplets of size around 200–300 µm.

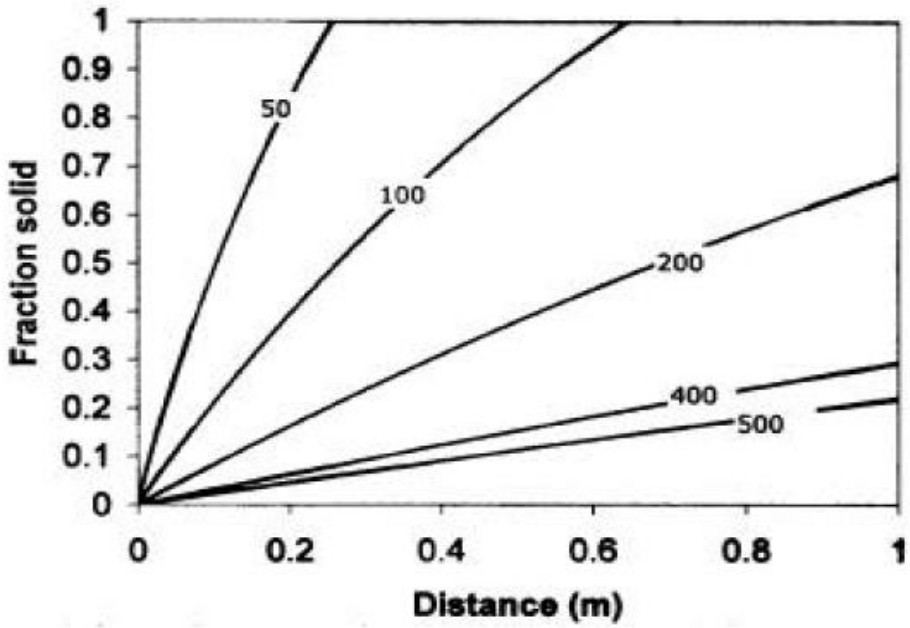

FIGURE 4.3 percentage of solid in the droplets versus flight distances

Figure 4.4 shows the rate of cooling in the droplets. From the figures it is evident that the cooling rate is very high for almost all the sizes of droplets. Cooling rate for smaller droplets were more as they lose heat faster.

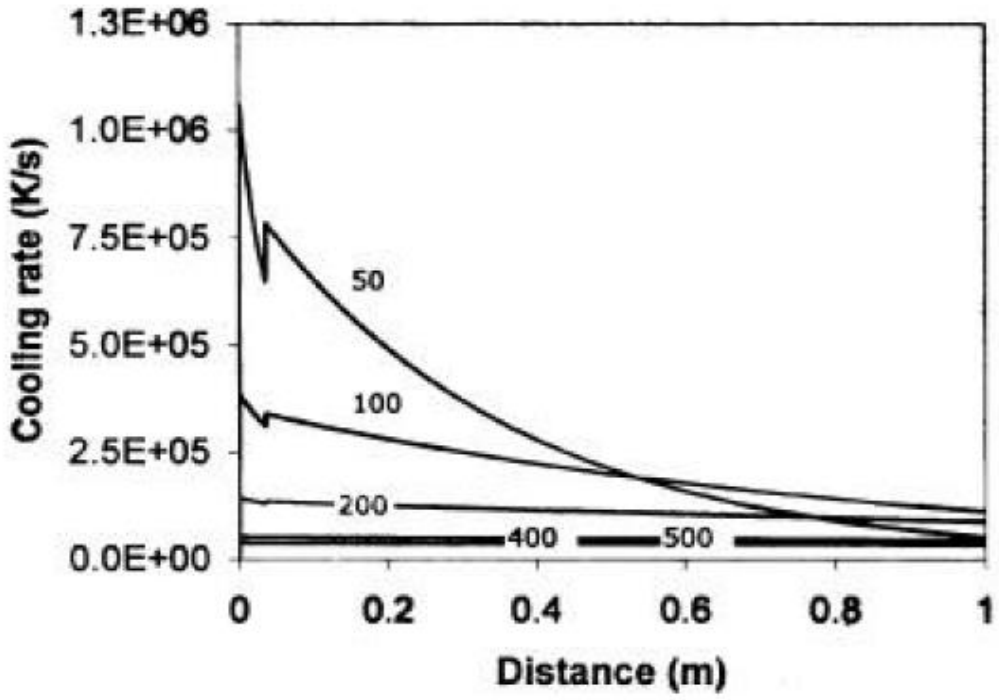

FIGURE 4.4 the rate of cooling in the droplets.

5. Solidifications of gas atomized droplets

Nucleation and growth of the crystal describes the solidification behavior of gas atomized droplets. Initially the solidification process is described by a homogeneous nucleation with slow cooling rates and thus without under-cooling for pure metals. Here it is implicit that the superheated melt droplet while cooling to the phase change temperature releases the latent heat and transfers it across the surface. After solidification the particle mass cools down further. In the heterogeneous cooling model the foreign particles initiate the cooling process. In this model, upon reaching the solidification temperature, a balance exists between the released latent heat and the heat convectively transferred across the surface of the droplet and thus the temperature of the droplet remains constant during solidification. These solidification models have been used in spray forming, for example, by **Zhang (1994) and Liu (1990)**.

The solidification model described here **(Bergmann, 2000)** was developed for low carbon steel C30 (0.30 wt. % C), but may be easily adapted to other material compositions.

The solidification model explained here is developed for low carbon steel C30 (0.30 weight% C) but is easily modified to other material compositions. Figure 2.10 shows part of the iron-carbon phase diagram, where the area for C30 is marked. For low cooling rates, temperature with respect to time curve can be drawn using this phase diagram. As in spray forming the cooling rate immediately after atomizations is very high hence there is a chances of undercooling even before the nucleation starts.

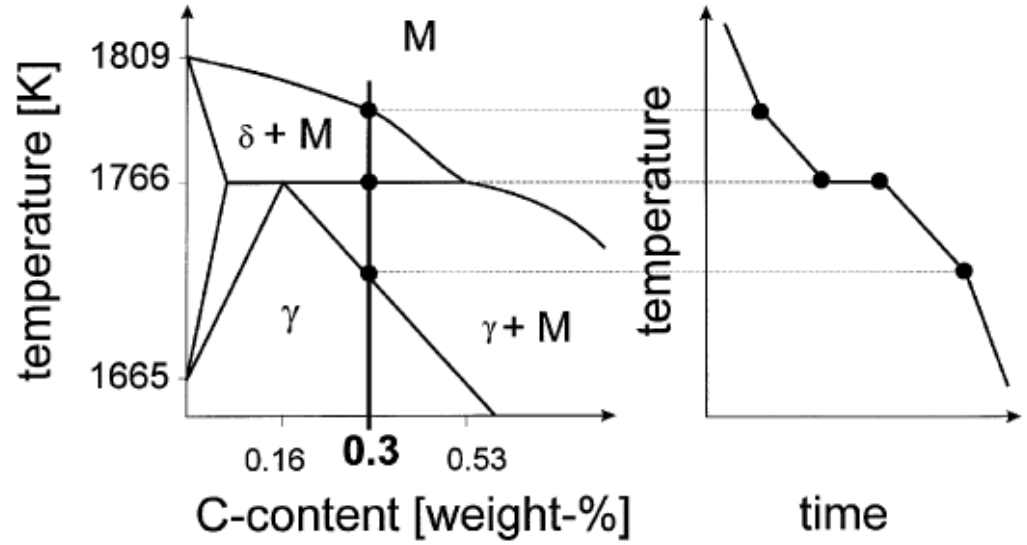

FIGURE 5.1 Phase Diagram of the Fe-C and the corresponding variation in phases with time

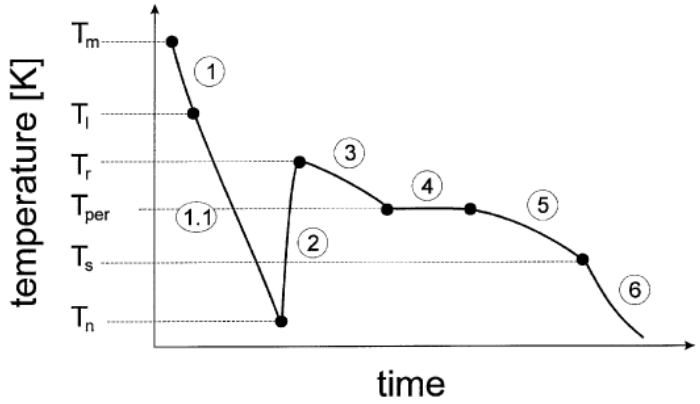

FIGURE 5.2 Temperature variation of gas atomized droplets with respect to time.

Starting with the superheated temperature T_m, the droplet cools down to liquidus temperature T_l. If the cooling rate is high droplet may undercool until nucleation starts on reaching the nucleation temperature. As there is release in latent heat of fusion during recalescence, the droplet temperature increases until it reaches a local maximum in the cooling curve at T_r. Later on it follows segregated solidification, as the temperature keeps on decreasing. At temperature T_{per}, the peritectic transformations takes place at constant droplet temperature. As the peritectic transformation ends up, segregated solidification starts again until the droplet is completely solidified at T_s. After this in solidified state itself the droplet cooling continues.

Separate analysis of droplet cooling and solidification:

6. Cooling in the liquid state

For a spherical droplet, the change of internal heat content according to convection and radiation heat transfer can be expressed by:

$$C_{d,l}\frac{dT_d}{dt} = -\frac{6h}{\rho_d d_d}(T_d-T_g) - \frac{6\varepsilon\sigma}{\rho_d d_d}(T_d^4-T_w^4) \qquad (6.1)$$

where T_d = droplet temperature, T_g = gas temperature and T_w = temperature of the surrounding walls. The specific heat capacity of the liquid droplet material is c_{dl}; h is the heat transfer coefficient, ε and σ are the emissivity and Stefan–Boltzmann constants, ρ_d and d_d are the droplet's density and diameter, respectively.

6.1 Undercooling:

The solidification process does not start immediately after liquidus temperature but the solidification depends on the cooling rate and on the size of the droplet. Nucleation temperature can be much lower than the liquidus temperature. The nucleation temperature for continuous cooling is defined as the temperature, where the number of nuclei N_n in the droplet volume V_d is identical to one:

$$N_n = V_d \int_{T_l}^{T_n} \frac{J(T)}{\dot{T}}\,dT = 1 \qquad (6.2)$$

Heterogeneous nucleation minimizes the degree of undercooling. The maximum undercooling for iron based alloys is 295 Kelvin and a minimum undercooling of 3 Kelvin is assumed.

6.2 Recalescence:

As the solidification starts there is an increase in the temperature of droplet due to release of latent heat of fusion. The conservation equation for the droplet thermal energy is extended to:

$$C_{d,l}\frac{dT_d}{dt} = \Delta h_f \frac{df_s}{dt} - \frac{6h}{\rho_d d_d}(T_d-T_g) - \frac{6\varepsilon\sigma}{\rho_d d_d}(T_d^4-T_g^4) \qquad (6.3)$$

where f_s as fraction solid (f_s = O droplet is completely liquid; f_s =1 droplet is completely solid) and the specific heat capacity of the droplets c_d as the average of the solid and liquid contents:

$$C_d = f_s C_{ds} + (1-f_s) C_{d,l} \qquad (6.4)$$

The phase of recalescence ends, when the production rate of internal heat equals the heat transfer from the droplets surface. Here, the cooling curve of a droplets reaches a local maximum and the droplet temperature equals T_r:

$$\Delta h_f \frac{df_s}{dt} = \frac{6h}{\rho_d d_d}(T_r-T_g) - \frac{6\varepsilon\sigma}{\rho_d d_d}(T_r^4-T_w^4) \qquad (6.5)$$

6.3 Segregated solidification 1:

The heat conservation equation in this stage is described by:

$$\frac{dT_d}{dt}\left(c_d+\Delta h_f \frac{df_s}{dT_d}\right) = \frac{6h}{\rho_d d_d}(T_d-T_g) - \frac{6\varepsilon\sigma}{\rho_d d_d}(T_d^4-T_w^4) \qquad (6.6)$$

6.4 Peritectic transformation:

When the droplet temperature reaches the peritectic temperature, it remains at a constant value until this phase transformation got completed. The change in solid fraction during peritectic solidification is described by:

$$\Delta h_f \frac{df_s}{dt} = -\frac{6h}{\rho_d d_d}(T_d-T_g) - \frac{6\varepsilon\sigma}{\rho_d d_d}(T_d^4-T_w^4) \qquad (6.7)$$

Peritectic solidification gets completed, when the composition of the remaining liquid reaches the appropriate concentration.

6.5 Segregated solidification 2:

Segregated solidification again come into picture after peritectic transformation.

6.6 Cooling in the solid state:

Further cooling of droplet takes place after solidification. This process can be evaluated from the following equation:

$$c_{ds}\frac{dT_d}{dt} = -\frac{6h}{\rho_d d_d}(T_d-T_g) - \frac{6\varepsilon\sigma}{\rho_d d_d}(T_d^4-T_w^4) \qquad (6.8)$$

with c_{ds} as the specific heat capacity of the solid materials.

7. Solidification behavior inside the melt particles

The temperature variation inside a single spherical droplet during solidification has been studied numerically by **Kallien (1988) and Hartmann (1990)**. The simulation program was developed for solidification during metals casting.

It includes undercooling thus calculates three-dimensional temperature variation in gas atomized droplet. The model is based on Fourier law for transient heat conduction in three-plane (Cartesian) coordinates as-:

$$\rho c_p \frac{\partial T}{\partial t} = \frac{\partial}{\partial x}\left(\lambda\frac{\partial T}{\partial x}\right)+\frac{\partial}{\partial y}\left(\lambda\frac{\partial T}{\partial y}\right)+\frac{\partial}{\partial z}\left(\lambda\frac{\partial T}{\partial z}\right) \qquad (7.1)$$

where conductivity λ, density ρ and heat capacity c_p, depend on location and temperature.

A modified temperature is introduced to achieve linear differentials equation:

$$\Theta=\frac{1}{\lambda_0}\int_0^T \lambda dT \qquad (7.2)$$

and thus linear differential equation was :

$$\frac{\rho c_p}{\lambda_0}\frac{\partial T}{\partial t} = \frac{\partial^2 \theta}{\partial x^2} + \frac{\partial^2 \theta}{\partial y^2} + \frac{\partial^2 \theta}{\partial z^2}$$

(7.3)

Finite difference method was used to solve this equation on an orthogonal-plane three dimensional grid.

The assumed boundary conditions are:

- The surrounding gas is assumed to be at constant temperature,
- Constant heat transfer coefficients across the whole surface of the droplet.
- At preselected nucleation temperature the solidification was initiated and nucleation was considered to take place at either at single point or at number of grid cells.

A six stages approach for the particle solidification was assumed:

(1) Cooling of the melts from superheating until the nucleation temperature is reached,

(2) Attaining the highest undercoolings,

(3) Solidification and recalescence,

(4) Cooling and solidification in the melt temperature range between solidus and liquidus,

(5) end of solidifications,

(6) Cooling of the solidified particles.

For the recalescence phase, the releasing velocity of latent heat depend on undercooling ΔT:

$v=K\Delta T$

As soon as the grid cells solidifies completely the adjacent cells begin to release the latent heat. Degree of undercooling controls the velocity of solidification.

The heat transfer coefficient was taken as h = 20 000 W/m^2 K and the undercooling prior to nucleations was considered to be 50 K.

The solidification process initiates at a single point on the surface of the particle in a plane inside the particles. As there is release of latent heat, the interior of the particle gets heated up. For a 10% solidification rate, movement of the solidification front is visible, which raises the temperature of the surrounding grid cells close to the liquidus temperature.

As Biot number is very less temperature variation inside the spherical droplets are neglected. Thus this behavior necessitates for refined modeling in order to obtain realistic spray formings modeling results.

Conclusion

It has been suggested in this paper that there are many reasons why a problem-solving approach can contribute significantly to the outcomes of a mathematics in spray formings. A problem solving approach can provide vehicle to researchers to construct their own ideas about mathematics and to take responsibility for their own learning. There is little doubt that the mathematics program can be enhanced by the establishment of an environment in which researchers are exposed to oppose to more traditional models of research about problem solving. The challenge for researchers at all levels, is to develop the process of mathematical thinking alongside the knowledge and to seek opportunities to solve spray formings tasks in problem-solving contexts.

REFERENCES:

1. Heat conduction by M. Necati Ozisik
2. Heat Transfer by J.P. Holman

3. N S Mahesh, Johnson Mendonca, M K Muralidhara, B K Muralidhara And C Ramachandra "Modeling of droplet dynamic and thermal behaviour during spray deposition",_ 2003.
4. Bergmann, D., Fritsching, U and Bauckhage, K. "A mathematical model for cooling and rapid solidification of molten metal droplets", *Int. J. Therm. Sci*.(2000)
5. Bergmann, D., Fritsching, U. and Bauckhage, K. "Simulation of molten metal droplet sprays", *Comp.Fluid Dynamics J.* (2001a)
6. Bergmann, D., Fritsching, U. and Crowe, C. T. "Multiphase flows in the spray forming process," *Proc. 2nd International Conference on Multiphase Flow*, 3–7 April, Kyoto.
7. Clift, R., Grace, J. R. and Weber, M. E. "*Bubbles, Drops and Particles"*, Academic Press, San Diego, CA (1978)
8. Crowe, C. T., Sharma, M. P. and Stock, D. E. "The particle-source-in-cell method for gas droplet flow", *J. Fluids Engng*. 99 (1977).
9. Crowe, C. T., Sommerfeld, M. and Tsuji, Y. "*Multiphase Flows with Drops and Particles"*, CRC Press, Boca Raton, CA (1998)
10. Fritsching, U., Liu, H. and Bauckhage, K. "Numerical modelling in the spray compaction process", *Proc.5th International Conference on Liquid Atomization and Spray Systems, ICLASS-91*, Gaithersburg, MD, NIST SP813 (1991)
11. Fritsching, U., Liu, H. and Bauckhage, K. "Two-phase flow and heat transfer in the metal spray compaction process", *Proc. International Conference on Multiphase Flows '91*, 24_7 September, Tsukuba (1991)
12. Grant, P. S., Cantor, B. and Katgerman, L. *Acta Metall. Mater*. 42 (1993)
13. Gutierrez-Miravete, M., Lavernia, E. J., Trapaga, G. M. and Szekely, J. "A mathematical model of the liquid dynamic compaction process", *Int. J. Rapid Solidification.* (1988)
14. Hartmann, G. C. (1990)
15. Lavernia, E. J., Gutierrez, E. M., Szekely, J. and Grant, N. J. "A mathematical model of the liquid dynamic compaction process and heat flow in gas atomization", *Int. J. Rapid Solidification* (1988).
16. Lawley, A., Mathur, P., Apelian, D. and Meystel, A. "Sprayforming: process fundamentals and control," *Powder Metall*. 34 (1990).
17. Lee, E. and Ahn, S. "Solidification progress and heat transfer analysis of gas atomized alloy droplets during spray forming", *Acta Metall. Mater*. 42 (1994) .
18. Levi, C. G. and Mehrabian, R. "Heat flow during rapid solidification of undercooled metal droplets", *Metall. Trans. A: Phys. Metall. Mater. Sci*. 13A (1982).
19. Mathur, P., Annavarapu, S., Apelian, D. and Lawley, A. "Process control, modeling and applications of spray casting", *J. Metals* 41 (1989b).
20. Mathur, P., Annavarapu, S., Apelian, D. and Lawley, A. "Spray casting: an integral model for process understanding and control", *Mater. Sci. Engng*. A142 (1991): 261–70
21. Mathur, P., Apelian, D. and Lawley, A. "Analysis of the spray deposition process", *Acta Metall*. (1989a) .
22. Ojha, S. N., Tripathi, A. K. and Singh, S. N. "Spray atomization and deposition of an Al–4Cu–20Pb alloy", *Powder Metall. Int.* 25 (1992).
23. Ottosen, P. "Numerical simulation of spray forming", PhD thesis, Technical University of Denmark, (1993)
24. Payne, R. D., Matteson, M. A. and Moran, A. L. "Application of neural networks in spray forming technology", *Int. J. Powder Metall*. 29 (1993)